Phonon transmission through a nonlocal metamaterial slab

Yi Chen[1*], Ke Wang[1,2], Muamer Kadic[3], Sebastien Guenneau[4], Changguo Wang[2], and Martin Wegener[1,5]

[1]Institute of Applied Physics, Karlsruhe Institute of Technology (KIT), Karlsruhe 76128, Germany.
[2]Center for Composite Materials, Harbin Institute of Technology, Harbin 150001, P.R. China.
[3]Institut FEMTO-ST, UMR 6174, CNRS, Université de Bourgogne Franche-Comté, Besançon 25030, France.
[4]UMI 2004 Abraham de Moivre-CNRS, Imperial College London, London SW7 2AZ, United Kingdom
[5]Institute of Nanotechnology, Karlsruhe Institute of Technology (KIT), Karlsruhe 76128, Germany.

*Correspondence to: yi.chen@partner.kit.edu (Y.C.)

Abstract:

Previous theory and experiment has shown that introducing strong (nonlocal) beyond-nearest-neighbor interactions in addition to (local) nearest-neighbor interactions into rationally designed periodic lattices called metamaterials can lead to unusual wave dispersion relations of the lowest band. For roton-like dispersions, this especially includes the possibility of multiple solutions for the wavenumber at a given frequency. Here, we study the one-dimensional frequency-dependent acoustical phonon transmission of a slab of such nonlocal metamaterial in a local surrounding. In addition to the usual Fabry-Perot resonances, we find a series of bound states in the continuum. In their vicinity, sharp Fano-type transmission resonances occur, with sharp zero-transmission minima next to sharp transmission maxima. Our theoretical discussion starts with a discrete mass-and-spring model. We compare these results with solutions of a generalized wave equation for heterogeneous nonlocal effective media. We validate our findings by numerical calculations on three-dimensional metamaterial microstructures for one-dimensional acoustical wave propagation.

Introduction

The wave properties of ordinary crystals are determined by the atoms forming the crystal as well as by their interactions. Likewise, the wave properties of rationally designed artificial periodic lattices called metamaterials[1-3] are determined by the interior of the metamaterial unit cells as well as by the interactions among the unit cells[4-6]. A bulk of literature has used the approximation of considering interactions among only the nearest neighbors[7-9]. Interactions beyond the nearest neighbors have been considered to test the validity of this approximation[10]. However, in metamaterials, the interactions beyond the nearest neighbors can be designed rationally and can be made strong[10-14]. This additional design freedom has lately been used to realize unusual dispersion relations of the lowest acoustic or elastic metamaterial band[15-18]. For example, the latter can resemble the unusual dispersion relation, $\omega(k)$, of sound waves in superfluid helium[19, 20] that starts with an angular frequency of the wave, ω, proportional to its wavenumber, k, followed by a maximum (the "maxon") and a minimum (the "roton") versus k[21, 22]. Such unusual phonon dispersion relations have been observed experimentally using three-dimensional macroscopic metamaterials for airborne sound at audible frequencies[17, 18] and using three-dimensional microstructured metamaterials for elastic waves at ultrasound frequencies[17].

However, structures and devices in applications usually exploit multiple dissimilar materials and the interplay between them and their interfaces. A paradigmatic textbook heterostructure geometry is a slab with thickness L of material A clad between two semi-infinite half spaces of material B. For usual local materials A and B, it is well-known that this setting leads to Fabry-Perot resonances connected to unity wave transmission, $|T(\omega)| = 1$, through the slab at particular angular frequencies $\omega = \omega_i$ of the incident wave[23]. At these particular frequencies, the phase that the wave accumulates in one round trip through the slab is an integer multiple of 2π. For a slab with a sufficiently large number of unit cells within, this condition translates into $2kL = n_i 2\pi$, where $k = k(\omega_i)$ is the single wavenumber in material A at the angular frequency ω_i and n_i is an integer. Fabry-Perot resonances with high quality factors have numerous applications, e.g., as optical filters or interferometry[24].

Here, we discuss the case that material A in the slab is replaced by a nonlocal metamaterial. At a given angular frequency ω, such medium generally supports more than a single wave mode with single wavenumber k. For different wavenumbers $k_j(\omega)$, with $j = 1, 2, \ldots N$, at a given angular frequency ω, the behavior is richer than for local material slabs. We start by discussing the problem using a previously introduced simple discrete one-dimensional (1D) mass-and-spring model[15]. Apart from the nearest-neighbor interactions via Hooke's springs, it contains N-th nearest-neighbor interactions with integer $N \geq$

2. Here, we emphasize the example of $N = 3$, which is the smallest N for which the roton-like minimum fully lies inside of the first Brillouin zone (for $N = 2$ it lies right at the Brillouin zone border). We find a series of sharp Fano-type resonances in the frequency-dependent transmission $|T(\omega)|$ in the frequency region for which multiple solutions $k_j(\omega)$ for the wavenumber exist. We show that the linewidth of the Fano-type resonances tends to zero towards special points in material-parameter space corresponding to bound states in the continuum (BIC)[25]. BIC physics in general, not related to beyond-nearest-neighbor interactions in periodic lattices, has a long history in acoustics[26], elasticity[27, 28], as well as optics[29, 30], and has recently attracted renewed attention in the metamaterials community[31]. We refer the reader to the review articles[25, 29] for an introduction to and comprehensive reviews of the BIC field. Next, we discuss the nonlocal slab transmission on the level of a 1D effective-medium approximation for the displacement field of the heterogeneous 1D mass-and-spring model, which leads to a phenomenological generalized wave equation containing spatial derivatives up to order $2N$. Finally, we present numerical calculations for three-dimensional nonlocal metamaterial microstructures for wave propagation along one direction, again showing BIC behavior.

Results and Discussion

Mass-and-spring model. Figure 1(a) illustrates the infinite one-dimensional mass-and-spring toy model that we have discussed previously[15]. Herein, identical masses m, periodically arranged with period or lattice constant a, are connected to their immediate neighbors along the x-axis on the left and on the right by linear elastic Hooke' springs with spring constant K_1. In this form (i.e., for $K_N = 0$), Fig. 1(a) corresponds to the paradigmatic one-dimensional model for acoustical phonons in usual local media as described in any solid-state-physics textbook[32]. For the nonlocal case, the masses in Fig. 1(a) are additionally connected to their N-th nearest neighbor on the left and on the right by Hooke's springs with spring constant K_N. Shown is the example of $N = 3$. This is the lowest integer for which roton-like dispersion relations[15] can occur within the first Brillouin zone of the model. For $N = 2$, the roton-like minimum is right at the boundary of the first Brillouin zone. Clearly, the model can be extended to contain multiple orders of beyond-nearest-neighbor interactions[33]. Here, for simplicity, we only consider nearest neighbors plus neighbors with $N = 3$. We will see that the resulting behavior of slabs is extremely rich and complex already. The beyond-nearest-neighbor springs in Fig. 1 are meant symbolically, an actual feasible realization is discussed in Section V.

As an example for $N = 3$, Fig. 1(b) shows a slab of relative thickness $L/a = 6$ of such nonlocal material clad between a local mass-and-spring model. The thinnest possible slab corresponds to $L/a = N$, for which only a single N-th nearest-neighbor spring is left. For simplicity and clarity, we depict and study in what follows the case that the lattice constant a, the masses m, and the spring constants K_1 are constant throughout the entire structure considered. We notice that, for a given well-defined integer ratio L/a, the left and right boundaries of the nonlocal slab in Fig. 1(b) cannot be defined unambiguously anymore. Six of the seven masses in the slab have only third-nearest-neighbor springs to one side. Further inside of the nonlocal slab (in Fig. 1(b) only the middle mass), the masses have long-range interactions to their left and to their right-hand side. For the phenomenological effective-medium description to be discussed below, this obvious fact means that the boundaries between the local and the nonlocal medium cannot be considered as being sharp or discontinuous anymore. The boundaries are rather smeared out, which is a direct consequence of the nonlocality of the slab. This simple observation will become important for an intuitive interpretation of our results and for the effective-medium description described below.

Before discussing the nonlocal slab, let us briefly recapitulate the expected transmission, $T(\omega)$, of a slab of a local material embedded in a different local material, at the real-valued angular frequency ω. We define the complex-valued transmission as the ratio of the transmitted displacement amplitude or output, u_{out}, and the displacement amplitude incident onto the slab, u_{in}, i.e.,

$$T(\omega) = \frac{u_{\mathrm{out}}}{u_{\mathrm{in}}}. \tag{1}$$

The phase of $T(\omega)$ clearly depends on at which lattice site exactly we take the incident and the transmitted displacement, respectively. This dependence drops out when considering the modulus, i.e., $|T(\omega)|$. Therefore, we consider $|T(\omega)|$ in what follows. As pointed out in the introduction, for a local slab in a local surrounding, $|T(\omega)|$ generally exhibits Fabry-Perot resonances with $|T(\omega_i)| = 1$ at particular angular frequencies ω_i which fulfill the standing-wave condition[23]

$$k(\omega_i)L = n_i\pi, \tag{2}$$

with integer n_i. Clearly, this reasoning implies that the slab contains sufficiently many unit cells, such that the wavenumber k can assume nearly any value. For these particular angular frequencies, the wave accumulates a phase in one round trip within the slab that is an integer multiple of 2π. For the special case that the impedances between the two materials are matched, we have $|T(\omega)| = 1$ for all angular frequencies.

Let us apply this intuitive reasoning to a nonlocal slab with sufficiently many unit cells inside. As we have shown previously[15] and as can be seen from roton-like dispersion relation shown in Fig. 2(a), one generally has three solutions (for $N = 3$) for each direction (left/right or $+k/-k$) for the (real part of the) wavenumber at a given angular frequency, i.e., $k(\omega_i) \rightarrow k_j(\omega_i)$ and $n_i \rightarrow n_{ij}$ with $j = 1,2,3$. Intuitively, a standing-wave condition Eq. (2) has to be fulfilled for each one of them simultaneously to obtain a "special" behavior of $|T(\omega)|$ at certain angular frequencies ω_i. Below, we will connect this "special" behavior to bound states in the continuum (BIC). For arbitrary parameter choices of m, K_1, K_3, and a, and hence arbitrary dispersion relations $\omega(k)$, it is unlikely that the condition Eq. (2) can be fulfilled three times simultaneously for any one angular frequency ω_i. However, as pointed out above (see Fig. 1(b)), the boundaries of the nonlocal slab are not sharp (see above discussion on Fig. 1(a)), and, hence, the effective slab thickness, L_j^{eff}, may be different from L in Eq. (2), i.e., we have to replace $L \rightarrow L_j^{\text{eff}}$ in Eq. (2). Together, we obtain

$$k_j(\omega_i) L_j^{\text{eff}} = n_{ij}\pi \, . \tag{3}$$

Unfortunately, there is no obvious and unambiguous way to calculate the effective slab thicknesses L_j^{eff} and thereby the special frequencies ω_i from Eq. (3) and the given dispersion relation $k(\omega)$. Nevertheless, this simple reasoning connects the textbook treatment of Fabry-Perot resonances for ordinary local slabs to the more unusual resonances in nonlocal slabs discussed in this paper.

Before we discuss the problem more rigorously, especially including the possibility of only a small number of unit cells within the slab, let us address a subtlety of the dispersion relation connected to the finite-thickness slab that turns out to be important for an intuitive interpretation of our results. For the infinitely extended periodic nonlocal mass-and-spring model (see Fig. 1(a)), Newton's law for the displacement u_l of the mass m at site l along the x-axis reads

$$m\frac{\partial^2 u_l}{\partial t^2} = K_1(u_{l+1} - 2u_l + u_{l-1}) + K_N(u_{l+N} - 2u_l + u_{l-N}), l = -\infty, \dots, 0, \dots + \infty. \tag{4}$$

Without further assumptions or approximations, the plane-wave ansatz $u_l = \tilde{u}\exp\left(i(kx - \omega t)\right)$, with $x = la$ and constant prefactor $\tilde{u}$, leads to the phonon dispersion relation $\omega(k)$ given by[15]

$$\omega^2(k) = \frac{4}{m}\left(K_1 \sin^2\left(\frac{ka}{2}\right) + K_N \sin^2\left(\frac{Nka}{2}\right)\right). \tag{5}$$

Clearly, when taking the square root on both sides of Eq. (5), we obtain two signs for ω. As usual, we follow the convention to consider positive (real parts of the) angular frequencies. For an infinite non-dissipative nonlocal medium, according to Bloch's theorem[32], the wavenumber must be real. However, for a finite-thickness nonlocal slab, the wavenumber is not necessarily real because evanescent modes may appear. For the considered transmission *Gedankenexperiment*, the angular frequency is purely real (by definition) and positive by convention. Nevertheless, we plot in Fig. 2 all mathematical solutions of Eq. (5) for the most general case of complex-valued k and complex-valued ω. Panel (a) is for a parameter set (see caption) for which $\mathrm{Re}(\omega)$ versus $\mathrm{Re}(k)$ shows a roton-like dispersion relation with a pronounced maximum and a pronounced minimum. Panel (b) is for a parameter set (see caption) for which $\mathrm{Re}(\omega)$ versus $\mathrm{Re}(k)$ shows no roton minimum in the phonon dispersion relation. Nevertheless, in Fig. 2(b), we still obtain three solutions (three modes) for the complex-valued wavenumber k for real and positive ω in the range of $\mathrm{Re}(k) > 0$. We repeat that $\mathrm{Im}(k) \neq 0$ indicates evanescent modes that drop out for an infinite medium, but that we have to consider for a finite-thickness nonlocal slab. For a local medium with $K_N = 0$, be it finite or infinite in thickness, this subtlety does not apply because $\mathrm{Im}(k) = 0$ holds true for any real-valued $\omega > 0$.

We note in passing that the behavior shown in Fig. 2 can be understood in terms of the roton minimum being an exceptional point[34-36]. In fact, any k-position of a minimum or maximum of $\omega(k)$ in the first Brillouin zone of any type of wave in any kind of lossless system is an exceptional point in the sense that two eigenmodes coalesce in both eigenvalues and eigenvectors for the angular eigenfrequency ω at the k-position of the maximum or minimum. At the position of a saddle point (see Fig. 2(b)), even three eigenmodes coalesce. This exceptional degeneracy is lifted as soon as one introduces a perturbation. It is also lifted as soon as one considers finite imaginary parts of k (i.e., evanescent waves). As a result, one black line emerges from the roton minimum for increasing imaginary part of the wavenumber in Fig. 2(a). In Fig. 2(b), two black lines emerge from the saddle point for $\mathrm{Im}(k) > 0$.

Next, we discuss solutions for $|T(\omega)|$ of the nonlocal slab. As our model contains no losses, the sum of kinetic and potential energy is conserved, and the reflectivity spectrum, $|R(\omega)|$, is directly connected to the transmission spectrum by the relation

$$|R(\omega)|^2 + |T(\omega)|^2 = 1. \tag{6}$$

This expression is only meaningful and valid for a local surrounding that supports only a single relevant mode (in either direction). This condition is automatically fulfilled for the discrete mass-and-spring model (cf. Fig. 1), but has to be taken with caution for the below approximate effective-medium description in which a very small but finite nonlocality needs to be added to the surrounding of the slab. We will come back to this point below.

To mathematically compute the transmission spectrum for the discrete model (see Fig. 1(b)), we proceed as follows. An incident wave with angular frequency ω impinges onto the slab from the left-hand side. We aim at computing the frequency-dependent reflection and transmission coefficients. We write the displacements corresponding to masses with label $l \leq 0$ (see Fig. 1(b)) as

$$u_l = u_{\mathrm{in}} \exp(ikla) + u_{\mathrm{ref}} \exp(-ikla), \tag{7}$$

where u_{in} indicates the complex-valued amplitude of the incident wave, k is the wavenumber, and u_{ref} represents the unknown amplitude of the reflected wave, respectively. To ease readability, the time harmonic factor $\exp(-i\omega t)$ is omitted here and throughout the following. It can be shown that the displacements of the masses with label $l \leq -1$ satisfy their balance equations automatically. Likewise, we represent the displacements of the masses with label $l \geq L/a$ by,

$$u_l = u_{\mathrm{out}} \exp(ik(l - L/a)a)\,, l \geq L/a \tag{8}$$

Here, u_{out} indicates the unknown amplitude of the transmitted wave. In total, we have $L/a + 1$ unknowns, including u_{ref}, u_{out}, and the displacements, u_l, with $l = 1, 2 \ldots (L/a - 1)$. These unknowns are obtained from $L/a + 1$ equilibrium equations for the masses with labels $l = 0, 2 \ldots L/a$. As defined above, the transmission coefficient is obtained via $T(\omega) = u_{\mathrm{out}}/u_{\mathrm{in}}$.

For example, for $L/a = 4$, we obtain the transmission spectrum

$$T(\omega) = \frac{2i\sin(ka)K_1^2(K_1(K_1+K_3)(K_1+5K_3) - 2K_3(4K_1+K_3)m\omega^2 + 2K_3m^2\omega^4)}{F_1(\omega)F_2(\omega)}. \tag{9}$$

Herein,

$$F_1(\omega) = \exp(ika)\,K_1(2K_1 + K_3 - m\omega^2) - (3K_1 - m\omega^2)(K_1 + 2K_3 - m\omega^2), \tag{10}$$

and

$$F_2(\omega) = 2(\exp(ika) - 1)K_1^3 + m^2\omega^4(M\omega^2 - 2K_3) + (\exp(ika) - 6)K_1 m\omega^2(M\omega^2 - K_3) +$$
$$K_1^2(9m\omega^2 - 2K_3 + 2\exp(ika)\,(K_3 - 2m\omega^2)). \tag{11}$$

The corresponding explicit expressions become very lengthy for slab length $L/a \geq 5$, and are hence not provided here.

Fig. 3(a) depicts an example of the calculated transmission $|T(\omega)|$ (gray scale) of the nonlocal slab (see Fig. 1(b)) versus ω and versus the spring-constant ratio K_3/K_1. For simplicity, all other model parameters are fixed (see caption). For reference, panel (b) shows the phonon dispersion relation for the slab for selected values of K_3/K_1 (see dashed lines). We find a complex behavior. In Fig. 3(a), for low frequencies, transmission peaks occur that follow the expectation for ordinary Fabry-Perot resonances (labelled "FP" in Fig. 3). At higher frequencies, near specific special frequencies (see arrows in Fig. 3(a)), the resonances in transmission become more and more narrow. Exactly at these special frequencies and spring constant ratio K_3/K_1, the resonances disappear. We interpret these special frequencies as being due to bound states in the continuum (BIC).

To test this interpretation, we have performed additional numerical calculations of the eigenfrequencies and eigenmodes of the slab alone, i.e., without the surrounding (not shown). We find eigenfrequencies, ω_{BIC}, for which the corresponding eigenmodes exhibit strictly zero displacement amplitude at the left and right end of the slab for all times t. Obviously, an incident plane wave with non-zero amplitude impinging from the surrounding cannot couple to such an eigenmode. Correspondingly, the lifetime of this mode is infinitely long – provided that friction plays no role, as implied in our model, see Fig. 1 or Eq. (4). This means that the special frequencies of BIC resonances only depend on the slab properties, but not on the properties of the surrounding. The same holds true for usual Fabry-Perot resonances.

To connect to our above intuitive discussion for sufficiently many unit cells within the slab, we can decompose the BIC modes of the slab corresponding to the BIC angular frequencies ω_i into the three ($j = 1, 2, 3$) eigenmodes with wavenumbers $k_j(\omega_i)$ of the nonlocal dispersion relation according to Eq. (5) to fulfill the three standing-wave conditions Eq. (3) simultaneously. However, the reverse is not true. Just any arbitrary linear combination of the three standing-wave solutions fulfilling Eq. (3) will generally not lead to a BIC mode as the displacement of the masses at the two ends of the slab is not necessarily strictly zero.

For special (small) integer values of the relative slab thickness L/a, the BIC resonance frequencies ω_{BIC} can be obtained analytically. We consider those $(1 + L/a)$ eigenfrequencies of the $(1 + L/a)$ coupled masses in the slab in Fig. 1(b) for which the corresponding eigenmode is such that the mass on the left-hand side and the right-hand side of the slab have strictly zero displacement amplitude at all times t (but the masses in between have nonzero amplitude). Such solutions occur only for special combinations of the three slab parameters m, K_1, and K_N. For any N and $K_N = 0$, BIC solutions do not occur for any value of L/a. For $K_N \neq 0$, $N = 3$ and $L/a = 3$ (i.e., only a single third-nearest-neighbor spring), a BIC does not occur either. The simplest non-trivial case is $N = 3$ and $L/a = 4$, for which we have only two third-nearest-neighbor springs in the slab. It is straightforward to obtain the eigenstates for this system composed of five coupled masses. By demanding that the displacements of the two masses on the left end and on the right end of this chain are zero for all times (see Supplementary Note 1), we obtain

$$(K_3/K_1)_{\mathrm{BIC}} = 1; \; \omega_{\mathrm{BIC}} = \sqrt{\frac{3K_3}{m}}. \tag{12}$$

For large relative slab thicknesses L/a we find BIC modes numerically as it seems hard to obtain closed analytical solutions.

For frequencies and parameters near but not identical to these BIC conditions, an incident propagating plane wave can couple to the resonance mode localized within the slab. The interference of a continuum of propagating modes and a spectrally-sharp localized mode is well known to give rise to Fano-type line shapes[37], the detailed form of which depends on the Fano coupling parameter. In Fig. 4(a), we show a zoomed-in view of one BIC point highlighted by the yellow box in Fig. 3(a). For K_3/K_1 values below the BIC points and with increasing angular frequency ω, we find a transmission dip (zero transmission) followed by a transmission peak (complete transmission), whereas for K_3/K_1 ratios above the BIC frequency, the sequence flips and we find a transmission peak followed by a transmission dip with increasing frequency. This behavior is more clearly seen from the selected cuts shown in Fig. 4(b) corresponding to three different K_3/K_1 values.

Further examples for other L/a, represented likewise in Fig. 3(a), are shown in Supplementary Figure 1. We find BIC modes even if only two third-nearest neighbor Hooke's springs are kept ($L/a = 4$ and $N = 3$, see Eq. (6)). In the opposite limit of a thick slab, $L/a \gg 1$ (see Fig. 1(b)), in which we expect that we can consider the slab as an effective medium, the BIC resonances survive as well. This brings us to a possible effective-medium description.

Effective-medium description. For an infinitely periodic nonlocal mass-and spring model and for $N = 3$, we have previously argued[17] that one gets the following general form for the displacement field $u = u(x,t)$ within the long-wavelength limit ($ka \to 0$)

$$m\frac{\partial^2 u}{\partial t^2} = A_2\frac{\partial^2 u}{\partial x^2} + A_4\frac{\partial^4 u}{\partial x^4} + A_6\frac{\partial^6 u}{\partial x^6}. \tag{13}$$

In a previous study[17], we have derived explicit expressions for the parameters A_2, A_4, and A_6. However, it should be noted that one gets different explicit expressions for A_2, A_4, and A_6 depending on which terms of the expansion one keeps. For example, even for the nearest-neighbor interactions alone (i.e., for $K_1 \neq 0$ and $K_3 = 0$) one can obtain finite terms for all three coefficients A_2, A_4, and A_6 in Eq. (13). Unless $K_1 \ll K_3$ (which does not hold true for the parameters considered in this paper), these terms are not negligible compared to the ones originating from the third-nearest-neighbor interactions. Therefore, we have assumed a phenomenological spirit and have considered the parameters A_2, A_4, and A_6 in the general form Eq. (13) as fit parameters when plotting the phonon dispersion relations as gray curves in Fig. 4B and 4D in Martínez et al.[17]. Further examples are given in Wang et al.[16].

If one wants to go beyond this phenomenological treatment, one would have to expand the finite differences on the right-hand side of Eq. (4) to yet much-higher orders of spatial derivatives than in Eq. (13) in order to quantitatively reproduce the results of the discrete mass-and-spring model. However, in this case, nothing is gained because the point of a meaningful effective-medium description is that it should be simpler than the underlying discrete model (or microstructure or atomic structure). Otherwise, one could rather continue working with the more complete discrete model.

We assume the same phenomenological spirit here. However, importantly, for the slab geometry of interest in this paper, the coefficients A_2, A_4, and A_6 are no longer constant versus the x-coordinate (see Fig. 1(b)). For this case of a heterogeneous nonlocal medium, it is straightforward to derive, starting from Eq. (4), the more general form

$$m\frac{\partial^2 u}{\partial t^2} = \frac{\partial}{\partial x}\left(A_2(x)\frac{\partial u}{\partial x}\right) + \frac{\partial^2}{\partial x^2}\left(A_4(x)\frac{\partial^2 u}{\partial x^2}\right) + \frac{\partial^3}{\partial x^3}\left(A_6(x)\frac{\partial^3 u}{\partial x^3}\right), \quad (14)$$

in the limit of $a \to 0$. The coefficients $A_2(x)$, $A_4(x)$, and $A_6(x)$ can be expressed by the model parameters $K_1(x)$, $K_N(x)$ and spatial derivatives up to third order thereof (see Supplementary Materials of Martínez et al.[17] for the case of constant coefficients). However, again, the expressions for $A_2(x)$, $A_4(x)$, and $A_6(x)$ depend on which terms of the expansion one keeps. If one considers the mathematically strict limit of $a \to 0$, one gets discontinuous steps of the coefficients $A_2(x)$, $A_4(x)$, and $A_6(x)$ at the interfaces of the slab, leading to diverging derivatives on the right-hand side of Eq. (14). One possible strategy to solve Eq. (14) with such discontinuous jumps of parameters is to introduce additional continuity conditions (as described for low-order differential equations in many textbooks[38]) or to treat the derivatives in a distributional sense[39]. However, in the current paper, we rather assume continuous coefficients as detailed below.

We rather make a second phenomenological assumption: We search for reasonable coefficients $A_2(x)$, $A_4(x)$, and $A_6(x)$ that lead to a behavior of the transmission $|T(\omega)|$ of the nonlocal slab that at least roughly qualitatively resembles the behavior we have found for the discrete mass-and-spring model shown in Fig. 3 or Fig. 4. By "reasonable", we mean that the dependencies $A_2(x)$, $A_4(x)$, and $A_6(x)$ must assume constant values far away from the interfaces. However, we must assume phenomenological shapes of the transition in the smeared-out interface regions (see above discussion on Fig. 1(b)).

Intuitively, the smearing out extends over a length scale Na given by the nonlocal interaction of order N. Furthermore, the coefficients $A_4(x)$ and $A_6(x)$ must be extremely small in the local surrounding. Conceptually, they should be zero in a local medium. However, mathematically, they cannot be strictly zero there, because this would again lead to discontinuous jumps and hence divergences of spatial derivatives when attempting to solve Eq. (14).

We do *not* expect a quantitative agreement with our results for the discrete heterogeneous mass-and-spring model (see, e.g., Fig. 3) because this form of a phenomenological effective-medium description does not even capture the dispersion relation of the nonlocal model quantitatively (see Figs. 4B and 4D in a previous study[17]). The asymptotics for $|k| \to \pi/a$ is incorrect, too[40]. Our effective-medium description can only capture roughly and qualitatively the fact that there is a roton minimum at a finite wavenumber within the first Brillouin zone. Nevertheless, we feel that it is interesting and relevant to identify a simple effective-medium description that can at least capture the existence of BIC behavior for nonlocal slabs.

To compute the transmission spectrum of a nonlocal slab according to Eq. (14) within the effective-medium description numerically, we proceed as follows. Figure 6(a) and (b) illustrate the discrete model and the corresponding continuum model. Here, $L = 9a$ serves as an example. In the discrete model (see Fig. 5(a)), all springs connecting two neighboring masses are the same. Therefore, we can naturally set $K_1(x) = 1$ in the continuum model. The spatial dependence of the non-local spring constant $K_3(x)$ needs to be manually constructed. We assume a smooth function for $K_3(x)$ in the region of $0 < x < 3a$, roughly corresponding to the boundary length scale of the discrete slab (compare Fig. 5(a) and (b)). Due to mirror symmetry of the discrete system, $K_3(x)$ for $L - 3a < x < L$ is obtained by symmetry. For the central part of the slab, i.e., $3a < x < L - 3a$, and the two surroundings to the left and right of the slab, i.e., $x < 0$ and $x > L$, $K_3(x)$ becomes constant. This constant is determined by the value of the graded profiles at $x = 0$ and $x = L$. The effective coefficients, $A_2(x)$, $A_4(x)$, and $A_6(x)$ of the continuum model are chosen phenomenologically as described above.

Now, we consider a plane wave with angular frequency ω incident onto the left interface of the slab. Since the surrounding has small but non-zero coefficients A_4 and A_6, three reflected modes exist, one with a real wavenumber, corresponding to a propagating mode, and two with complex wavenumbers, denoting evanescent modes that exponentially decay away from the interface. The total displacement field can be written as

$$u(x) = u_{\text{in}} \exp(ikx) + R_1 \exp(-ik_1 x) + R_2 \exp(-ik_2 x) + R_3 \exp(-ik_3 x), x \leq 0. \qquad (15)$$

The wavenumber k_1 is purely real, while k_2 and k_3 should have positive imaginary parts to ensure exponential decay for $x < 0$. The three wavenumbers all satisfy the dispersion relation

$$\omega^2 = A_2 k_i^2 - A_4 k_i^4 + A_6 k_i^6 \tag{16}$$

for $i = 1, 2, 3$. In the transmission region, we start from the displacement field

$$u(x) = T_1 \exp(ik_1 x) + T_2 \exp(ik_2 x) + T_3 \exp(ik_3 x)\,, x \geq La. \tag{17}$$

Here, the three wavenumbers k_i, $i = 1, 2, 3$ are the same as in Eq. (15). In the above two expressions, R_i and T_i, $i = 1, 2, 3$, are the corresponding unknown reflection and transmission coefficients for the three modes.

To solve the six unknown coefficients, R_i and T_i, $i = 1, 2, 3$, wave propagation inside the non-local slab must be considered. However, due to inhomogeneous material parameters, the displacement fields cannot be constructed analytically. Here, we implement a state-space approach for solving the high-order ordinary differential equation[41].

We first re-write the above sixth-order ordinary differential equation (14) into the following matrix form,

$$\frac{\mathrm{d}\mathbf{S}(x)}{\mathrm{d}x} = \mathbf{P}(x) \cdot \mathbf{S}(x), \tag{18}$$

$$\mathbf{S}(x) = \begin{pmatrix} u(x) \\ A_2(x)u'(x) \\ A_4(x)u''(x) \\ A_6(x)u'''(x) \\ \left(A_6(x)u'''(x)\right)' + A_4(x)u''(x) \\ \left(A_6(x)u'''(x)\right)'' + \left(A_4(x)u''(x)\right)' + A_2(x)u'(x) \end{pmatrix}, \tag{19}$$

$$\mathbf{P}(x) = \begin{pmatrix} 0 & \frac{1}{A_2(x)} & 0 & 0 & 0 & 0 \\ 0 & \frac{A_2'(x)}{A_2(x)} & \frac{A_2(x)}{A_4(x)} & 0 & 0 & 0 \\ 0 & 0 & \frac{A_4'(x)}{A_4(x)} & \frac{A_4(x)}{A_6(x)} & 0 & 0 \\ 0 & 0 & -1 & 0 & 1 & 0 \\ 0 & -1 & 0 & 0 & 0 & 1 \\ -m\omega^2 & 0 & 0 & 0 & 0 & 0 \end{pmatrix}. \tag{20}$$

Here, the prime symbol $'$ represents the spatial derivative with respect to the coordinate x and $\mathbf{S}(x)$ is called the state-space vector.

Next, the slab is discretized into many thin layers. The left location and right location of the j^{th} layer are denoted as x_{j-1} and x_j, respectively. Each layer is assumed to be homogeneous with its material parameters being evaluated at its middle, i.e., $A_2\left(\left(x_{j-1}+x_j\right)/2\right)$, $A_4\left(\left(x_{j-1}+x_j\right)/2\right)$, and $A_6\left(\left(x_{j-1}+x_j\right)/2\right)$, respectively. The discretized problem will converge to the original problem with graded material parameter distribution if the discretized layers are sufficiently thin.

Within the j^{th} layer, the matrix $\mathbf{P}(x)$ becomes a constant matrix and the Eq. (19) has an exponential solution[41]. Furthermore, the two state-space vectors at both ends of the thin layer have the following transfer relation,

$$\mathbf{S}\left(x_j\right)=\mathbf{t}\left(x_j\right)\cdot\mathbf{S}\left(x_{j-1}\right), j=1,2\ldots, \tag{21}$$

with

$$\mathbf{t}\left(x_j\right)=\exp\left(\left(x_j-x_{j-1}\right)\mathbf{P}\left(\frac{x_{j-1}+x_j}{2}\right)\right). \tag{22}$$

Note that the state-space vector is continuous across the interface between two adjacent thin layers. Therefore, we can apply the transfer relation Eq. (21) sequentially to obtain the transfer relation between the two state space vectors at both ends, i.e., $x=0$ and $x=La$, of the slab region,

$$\mathbf{S}(La)=\mathbf{T}\cdot\mathbf{S}(0), \mathbf{T}=\prod_j \mathbf{t}\left(x_j\right). \tag{23}$$

The two state-space vectors $\mathbf{S}(La)$ and $\mathbf{S}(0)$ are also obtained from the derived displacement fields Eqs. (21) - (22) for the incidence region and transmission region. Together with the transfer relation Eq. (23), the six unknown coefficients, R_i and T_i, $i=1,2,3$ can be obtained.

In Fig. 6(a), we show the numerically calculated transmission results by using the above effective-medium model for a slab with relative length $L/a=9$. The other chosen parameters are given in the figure caption. By comparing Fig. 3(a) and Fig. 6(a), we see that the effective model can capture the BIC behavior as well as the usual Fabry-Perot resonance qualitatively well. The BIC behavior also occurs in the frequency range where multiple eigenstates coexist (the roton part of the dispersion relation). The agreement with respect to the discrete model cannot be quantitative because the dispersion relations for the discrete model and the effective-medium model do not match exactly (Fig. 6(b)). As for previous discrete model (see Fig. 4), Figure 7 shows an enlarged view of the BIC point enclosed by the yellow box in Fig. 6(a). While the BIC point appears in both, Fig. 4(b) and Fig. 7(b), the transmission line shapes are qualitatively different. Results for different relative slab thicknesses in the effective-medium model are shown in Supplementary Figure 2. There, one can again see the trend that, as the slab thickness increases, more and more BIC points appear.

Metamaterial microstructures. So far, we have only considered a conceptual discrete mass-and-spring toy model and an effective-medium simplification thereof. This model itself can hardly be called a metamaterial. We have previously discussed that acoustic metamaterials for airborne sound can be described approximately by the mass-and-spring toy model[16]. Therefore, in this section, we perform numerical calculations for a slab of a specific acoustic metamaterial.

Figure 8(a) illustrates the considered metamaterial for airborne sound. The metamaterial is composed of acoustical cavities (blue cylinders) and acoustical tubes (green and red pipes). Based on our previous theoretical and numerical studies[16], the acoustical cavities can be treated as masses in the discrete model in Fig. 1(a), and the green (red) acoustical tubes correspond to nearest-neighbor (third-nearest-neighbor) springs. The ratio between the strength of the third-nearest-neighbor interactions and that of the nearest-neighbor interactions can be tuned through the geometry parameter R_3/R_1. The metamaterial structure shown in Fig. 10(a) forms the basis for the following calculations. Figure 8(b) exhibits a specific realization of the discrete model in Fig. 1(b) by using the illustrated nonlocal metamaterial in Fig. 8(a). The length of the metamaterial structure in Fig. 8(b) is about $L = 5a$. The surrounding tubes have no cut-off frequency, which is similar to the continuum model in the preceding section. Viscosity of air usually leads to losses in acoustic systems[42] and can influence the high-quality-factor resonances near the expected BIC points. Therefore, in what follows, we will show and discuss numerical results with and without losses.

We simulate the sound wave propagation in the metamaterial shown in Fig. 8(b) by using the commercial software COMSOL Multiphysics. A plane-wave radiation condition is applied at the bottom of the model to mimic an incident plane wave. A perfectly matched layer is employed at the top to mimic a semi-infinite transmission region with no reflections[43]. All other boundaries are treated as acoustic rigid boundaries[23]. The linear acoustic equation in frequency,

$$\nabla \cdot (\nabla p_\omega(\mathbf{r})) = -\frac{\omega^2}{c_{\mathrm{air}}^2} p_\omega(\mathbf{r}) \tag{24}$$

is solved with the above specified boundary conditions. ω again represents the excitation angular frequency, $p_\omega(\mathbf{r})$ is the corresponding pressure field, and c_{air} is the speed of sound wave in air. The transmission coefficient T is extracted from the pressure field in the transmission region.

Results for the transmission behavior of the lossless microstructured slab are given in Fig. 9. Panel (a) depicts the transmission amplitude $|T|$ versus the wave frequency ω and the geometry parameters R_3/R_1. Panel (b) exhibits the calculated lowest phonon band for the periodic metamaterial in Fig. 9(a) for different ratios R_3/R_1. In the numerical simulations, we fix the radius $R_1 = 0.1a$ and vary the parameter R_3. In analogy to the above mass-and-spring model and continuum model, Fabry-Perot resonances are observed in Fig. 9(a). Furthermore, a BIC behavior is clearly identified within that frequency range, for which multiple Bloch wave modes coexist. Near by the BIC point, very sharp Fano resonances appear – as for the discrete model as well as for the effective-medium model (see above).

In Fig. 10, we show the calculated transmission amplitude $|T|$ as in Fig. 9(a), but with losses accounted for. Here, viscous damping in the acoustic pipes is treated *via* the "narrow region acoustics" in COMSOL Multiphysics. A quasi-BIC behavior is still observed from the plot. Here, the resonances near the BIC points have much smaller quality factors compared to the lossless case in Fig. 10(a). Nevertheless, the behavior is qualitatively similar to that of the discrete model and that of the effective-medium model, respectively.

We expect that our findings for nonlocal elastic slabs can be translated to other systems. For example, a thin film of superfluid helium, for which rotons were originally discovered, in a local surrounding should show a similar overall transmission behavior according to our intuitive interpretation. The detailed mathematical description might be quite different though. Furthermore, the nonlocal discrete mass-and-spring model discussed here can be exactly mapped onto an electrical circuit composed of lumped capacitors and inductors, where the capacitors correspond to the masses and two types of inductors to the nearest-neighbor and beyond-nearest-neighbor Hooke's springs, respectively.

Finally, we note again that the minimum in the roton-like dispersion relation corresponds to an exceptional point. Furthermore, we have shown that the roton-like dispersion relation leads to BIC for a nonlocal metamaterial slab. This BIC behavior has already occurred at frequencies near to those of the roton minimum of the slab. We speculate that further interesting behavior might occur if one tunes the system parameters such that the BIC frequency coincides with that of the roton exceptional point.

Data availability

The data that support the plots within this paper and other findings of this study are published on the open access data repository of the Karlsruhe Institute of Technology (https://doi.org/10.35097/860).

Code availability

The numerical simulations in this work for the mass-and-spring model have been performed by using the commercial software MATLAB. Numerical simulations for the elastic metamaterials are performed using the commercial software COMSOL Multiphysics. The code and models are published on the open access data repository of the Karlsruhe Institute of Technology (https://doi.org/10.35097/860).

Acknowledgements

We acknowledge support by the Deutsche Forschungsgemeinschaft (DFG, German Research Foundation) under Germany's Excellence Strategy via the Excellence Cluster "3D Matter Made to Order" (EXC-2082/1-390761711), by the Carl Zeiss Foundation through the "Carl-Zeiss-Foundation-Focus@HEiKA", by the Helmholtz program "Materials Systems Engineering", by the Alexander von Humboldt Foundation (Y.C.), and by the China Scholarship Council (K.W.).

Author contributions

Y.C. and K.W. performed the numerical simulations. K.W. and M.K. designed the metamaterials. Y.C. and S.G. developed the theory. M.W. wrote the first draft. C.W. and M.W. supervised the effort. All authors discussed the results and contributed to the writing and reviewing of the manuscript.

Competing interests

All authors declare no competing interests.

Figures and Captions

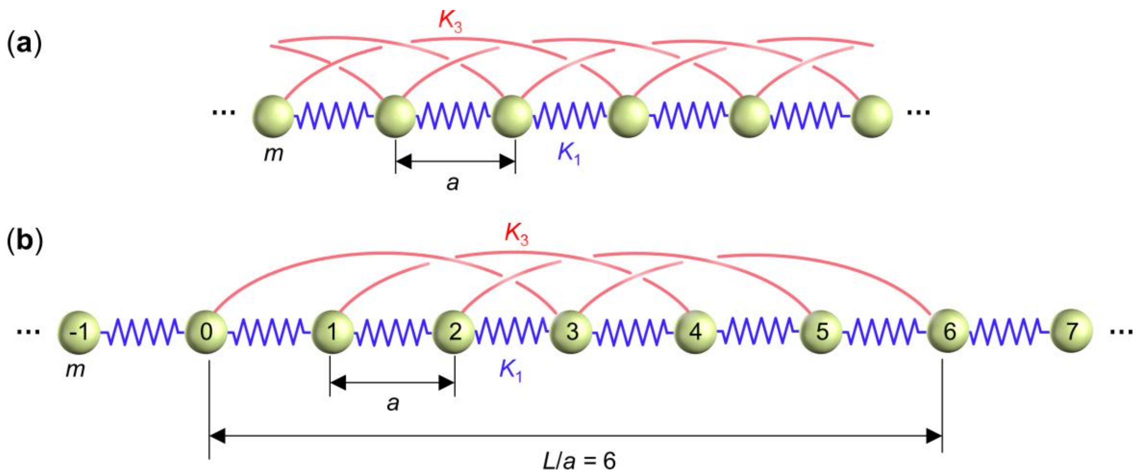

Figure 1. Illustration of mass-and-spring model. (a) An infinite periodic one-dimensional mass-and-spring model composed of masses (light yellow), m, connected to their nearest neighbors by Hooke's springs (blue) with spring constant K_1 and additionally connected to their N-th nearest neighbors by Hooke's springs (red) with spring constant K_N. Shown is the example of $N = 3$, which we emphasize in this paper because it is the smallest integer for which one obtains a roton-like minimum inside of the first Brillouin zone. The lattice constant is a. (b) A slab of such nonlocal material clad between half spaces of an ordinary local mass-and-spring model with only nearest-neighbor interactions. The slab thickness is defined by the integer ratio L/a. Shown is the example of $L/a = 6$ and $N = 3$. Note that the boundaries of the slab are smeared out in the sense that only the center mass out of the $(1 + L/a)$ masses in the slab has two third-nearest-neighbor connections. The remaining six masses have only one such connection. This smearing-out is an immediate consequence of the nonlocality.

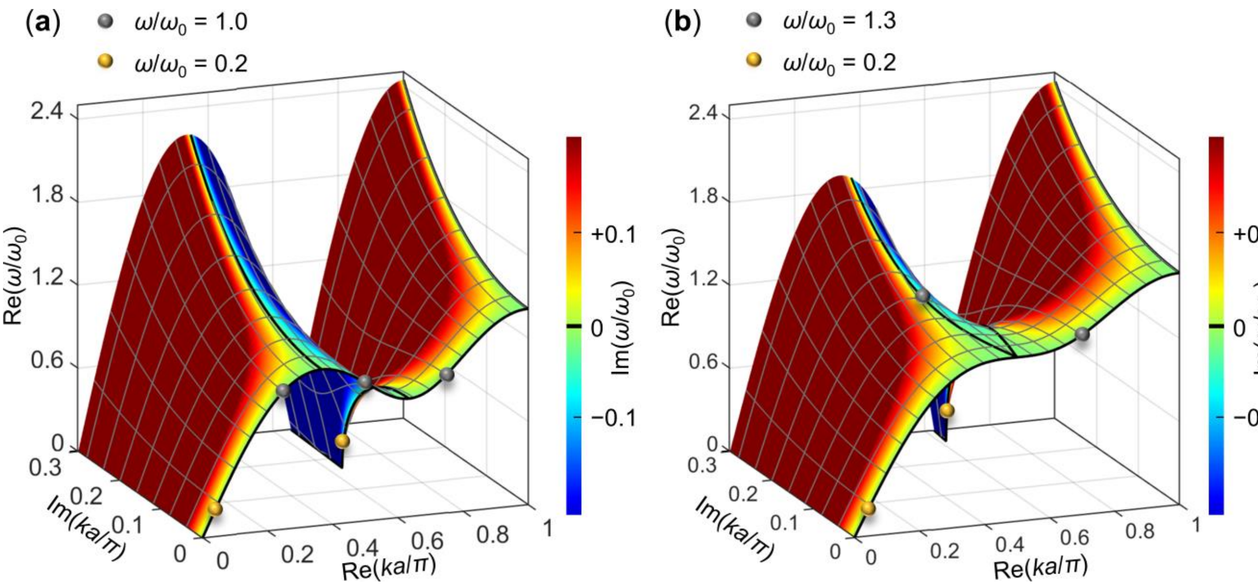

Figure 2. Dispersion relations of the mass-and-spring model. (a) Surface plot of real component of frequency ω versus the real and the imaginary components of the wavenumber k following Eq. (5). For the conditions discussed in this paper, the angular frequency ω is purely real. The wavenumber k is also purely real for a Bloch-periodic solution of an infinite periodic model. For a finite-thickness slab (see Fig. 1(b)), evanescent modes can play a role and the imaginary part of k is generally not zero. The imaginary part of the complex-valued angular frequency ω is shown by the false-color scale. Only the positive parts of the real and imaginary components of the wavenumber are shown here as the corresponding negative parts can be obtained by mirror symmetry. The four highlighted black lines on the surface lead to purely real angular frequency ω. Among them, one corresponds to purely real wavenumber and the other three correspond to complex wavenumbers in the range of $\mathrm{Re}(k) > 0$. For a normalized frequency of $\omega/\omega_0 = 1.0$, in between the local maximum and roton minimum, three real wavenumbers (see the three gray dots) can be obtained from the dispersion relation. For $\omega/\omega_0 = 0.2$ below the roton minimum, a real wavenumber and a pair of complex conjugate wavenumber are obtained (see two yellow dots). Parameters are $K_3/K_1 = 1.0$ and the normalization frequency is $\omega_0 = \sqrt{4K_1/m}$. (b) Parameters corresponding to the critical case without roton minimum in the dispersion relation, i.e., $m = 1$ and $K_3/K_1 = 1/3$. Note that still three solutions for the complex-valued k in the range of $\mathrm{Re}(k) > 0$ occur at a given angular frequency ω.

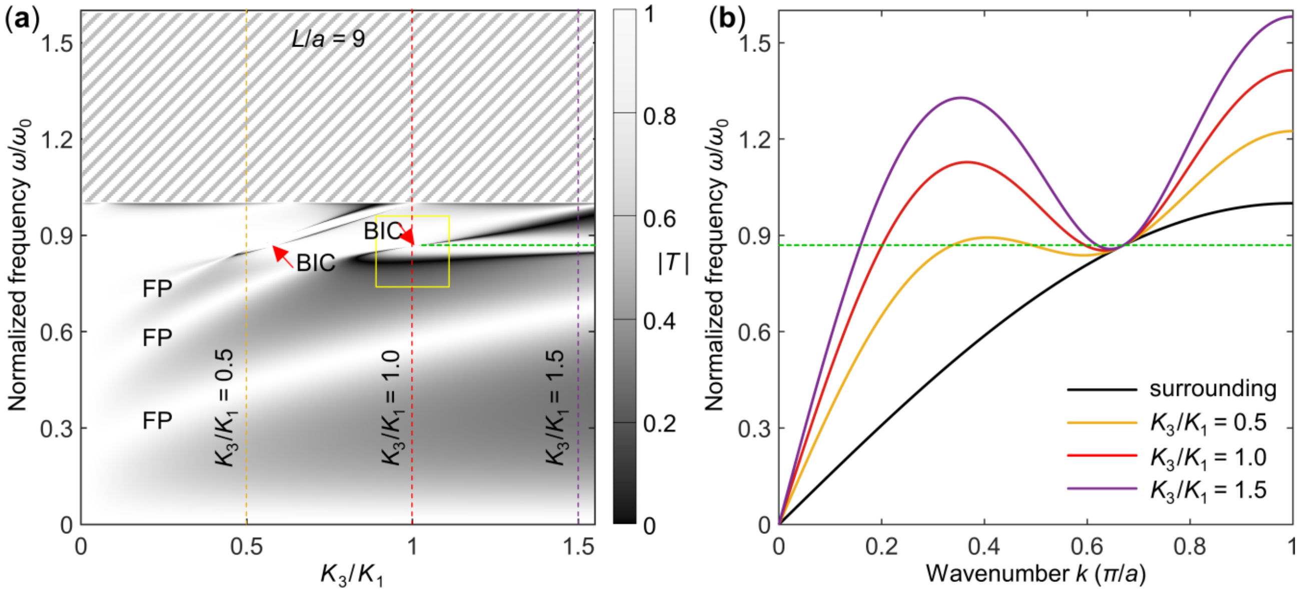

Figure 3. Phonon transmission results of the mass-and-spring model. (a) Calculated transmission amplitude $|T(\omega)|$ of the discrete nonlocal mass-and-spring-model slab (see Fig. 1(b)) shown on a gray scale versus ω and K_3/K_1. In the hatched region above the cut-off frequency $\omega/\omega_0 = 1.0$, waves cannot propagate in the surrounding medium. “FP” denotes Fabry-Perot resonances, “BIC” bound-states-in-the-continuum points. Note the Fano-type line shapes of $|T(\omega)|$ near the BIC points. Two “BIC” points are indicated. A zoom into one of them (see yellow box) is shown in Fig. 4(a). The normalization frequency is $\omega_0 = \sqrt{4K_1/m}$. Parameters are: $m = 1$, $L/a = 9$. (b) Illustration of the corresponding dispersion relations of the slab region for purely real ω and purely real k for different ratios of K_3/K_1.

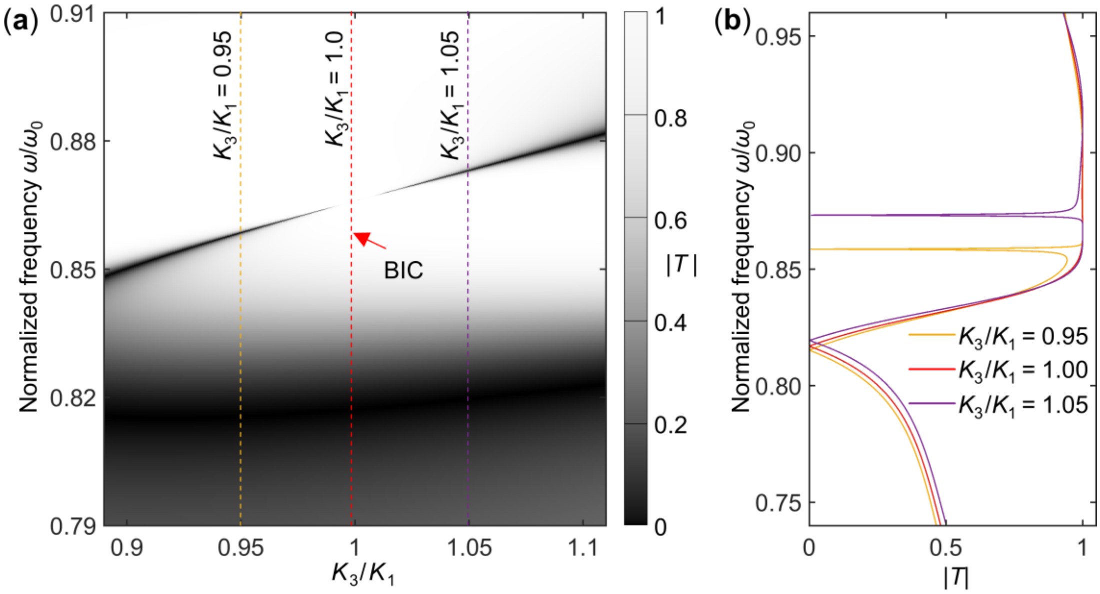

Figure 4. Zoomed-in view of the BIC and sharp resonances. (a) Zoomed-in view of the bound-states-in-the-continuum (BIC point) highlighted by the yellow box in Fig. 3(a). (b) Cuts through the data in panel (a) at three selected ratios K_3/K_1 (see dashed vertical lines in (a)). Extremely sharp resonance versus frequency ω occur for parameters close to the BIC point (yellow and purple curves). At the BIC point (red curve), the sharp resonance disappears as incident waves strictly do not couple to the BIC.

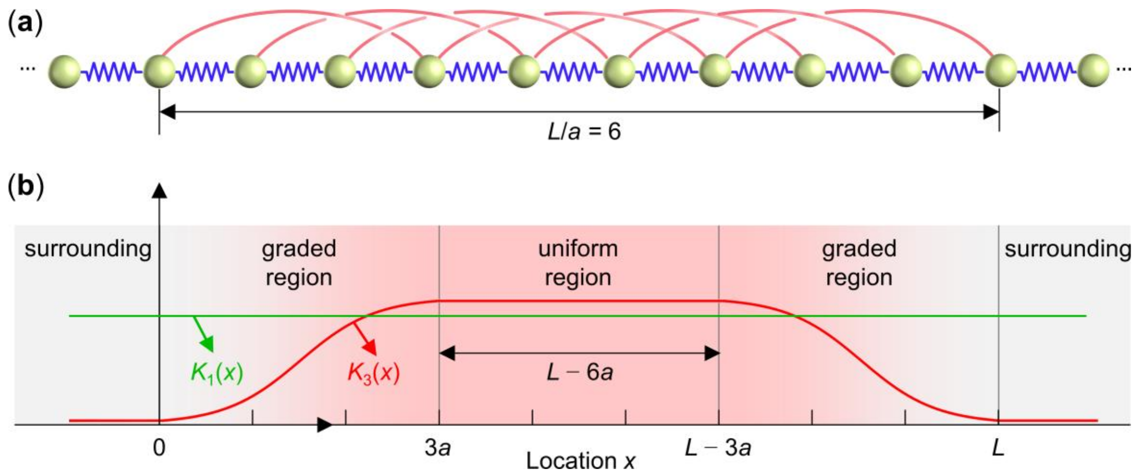

Figure 5. Illustration of the effective-medium model. (a) Discrete system with slab thickness L. $L = 9a$ is used as an example. (b) Scheme of the continuum model composed of the slab region and the two semi-infinite surroundings. The slab is further decomposed into a central uniform region, i.e., $3a < x < L - 3a$, and two graded regions, i.e., $0 < x < 3a$, and $L - 3a < x < L$. The graded regions represent smooth transitions of the effective parameters to those in the two surroundings. In the region of $0 < x < 3a$, a function that increases smoothly from an extremely small value to a finite value is assumed for $K_3(x)$, indicating the third-nearest-neighbor constants. $K_3(x)$ for $L - 3a < x < L$ is obtained from mirror symmetry of the system. For the central uniform part of the slab, i.e., $3a < x < L - 3a$, and the two surroundings, i.e., $x < 0$ and $x > L$, $K_3(x)$ becomes constant and is obtained from continuity. The parameter $K_1(x)$ is assumed to be constant throughout the 1D system, $K_1(x) = 1$. The effective parameters of the continuum model are constructed from the two spring constants $K_1(x)$ and $K_3(x)$, i.e., from $A_2(x) = K_1(x) + 9K_3(x)$, $A_4(x) = 6K_3(x)$, and $A_6(x) = K_3(x)$, respectively.

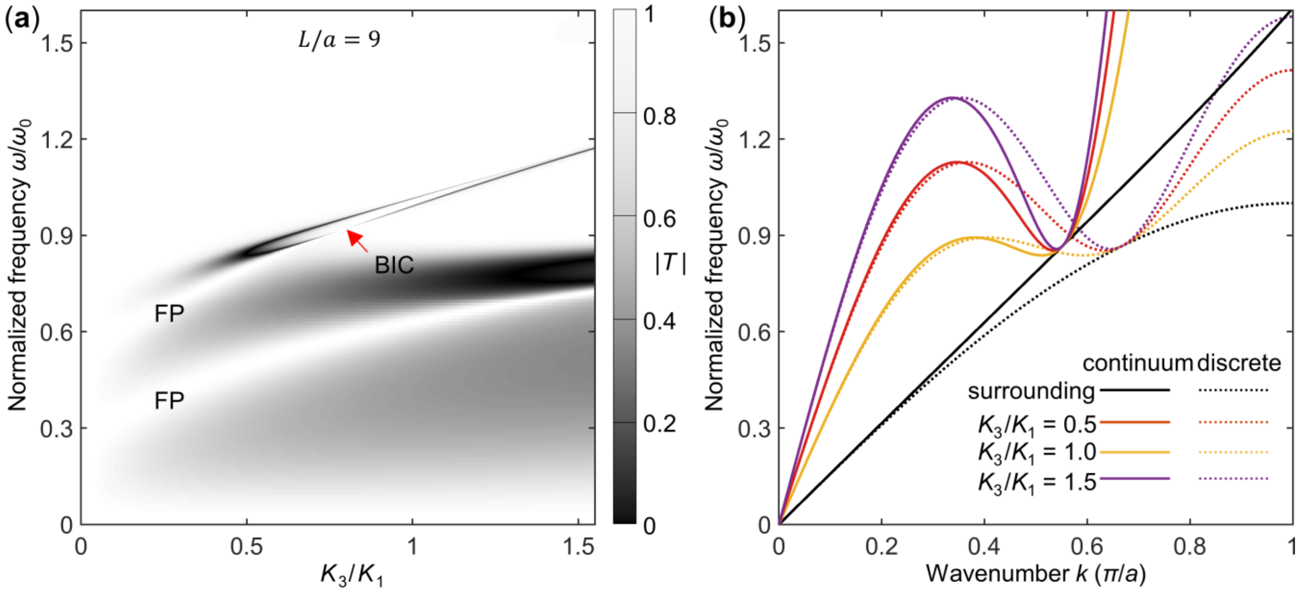

Figure 6. Phonon transmission results for the phenomenological effective-medium model rather than the discrete mass-and-spring model. (a) Phonon transmission results. Parameters are $L = 9a$ and $K_3(x)/K_1 = 1 - 1/\big(1 + \exp\big(2(x - 3a/2)\big)\big)$ for $0 < x < 3a$. The assumed $K_3(x)$ ensures that the two surrounding regions exhibit extremely small non-local stiffness parameters (about two orders of magnitude smaller than for the slab). (b) Dispersion relations for the effective-medium model (solid curves). The dashed curves correspond to the data in Fig. 3(b) for the discrete mass-and-spring model and can be compared directly to the effective-medium model.

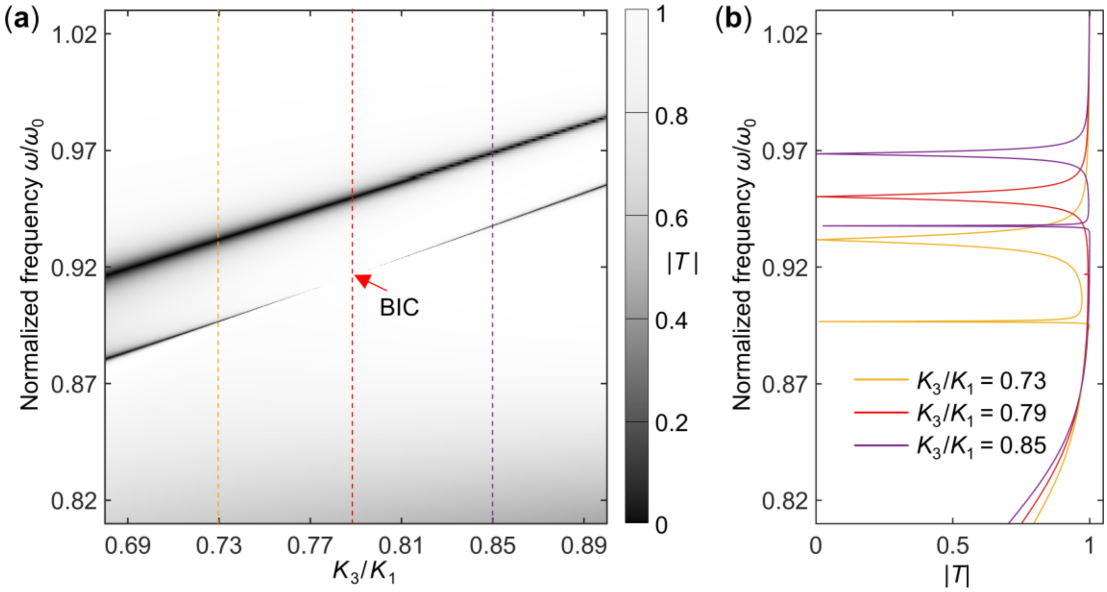

Figure 7. Zoomed-in view of the BIC and sharp resonances. (a) Zoomed-in view of the bound-states-in-the-continuum (BIC) point highlighted by the yellow box in Fig. 6(a). (b) Cuts through the data in panel (a) at three selected ratios K_3/K_1 (see dashed vertical lines in (a)).

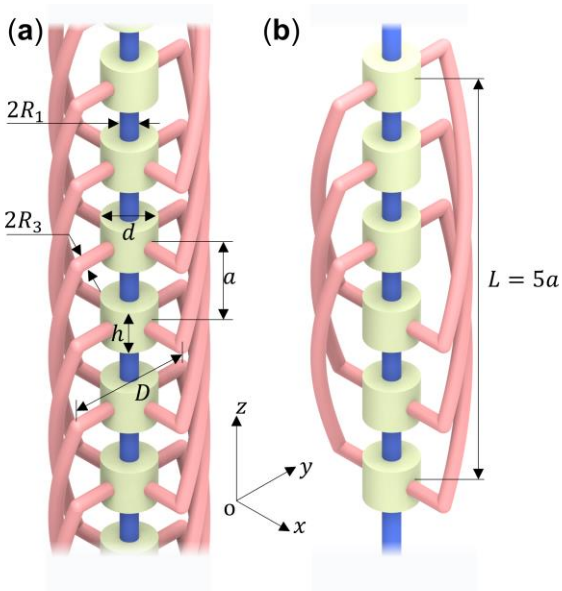

Figure 8. Illustration of the considered 3D acoustical metamaterial for airborne sound. (a) Infinite periodic metamaterial with non-local interactions. The metamaterial is composed of acoustical cavities (yellow cylinders) and acoustical channels (blue and red pipes). Colors are for illustration only, all parts represent voids for air. The yellow cylinders, with height h and diameter d, correspond to masses in the discrete mass-and-spring model, and the blue (red) pipes, with diameter $2R_1$ ($2R_3$), represent the nearest-neighbor interactions (third-nearest-neighbor interactions). The helix part of the red pipes has a major radius, $D/2$. (b) A specific realization of the discrete model in Fig. 1(b) by using the metamaterial structure in (a). The two semi-infinite pipes at both ends represent the surrounding. Therefore, the surrounding medium has no cut-off frequency, analogous to the effective-medium model shown in Fig. 6. Geometry parameters are: $h = 0.5a$, $d = 0.6a$, $D = 1.5a$, $R_1 = 0.1a$, and $a = 0.1$ m, respectively. For air, we choose the sound velocity $c_{\mathrm{air}} = 343\ \mathrm{m\ s^{-1}}$ and the mass density $\rho_{\mathrm{air}} = 1.29\ \mathrm{kg\ m^{-3}}$.

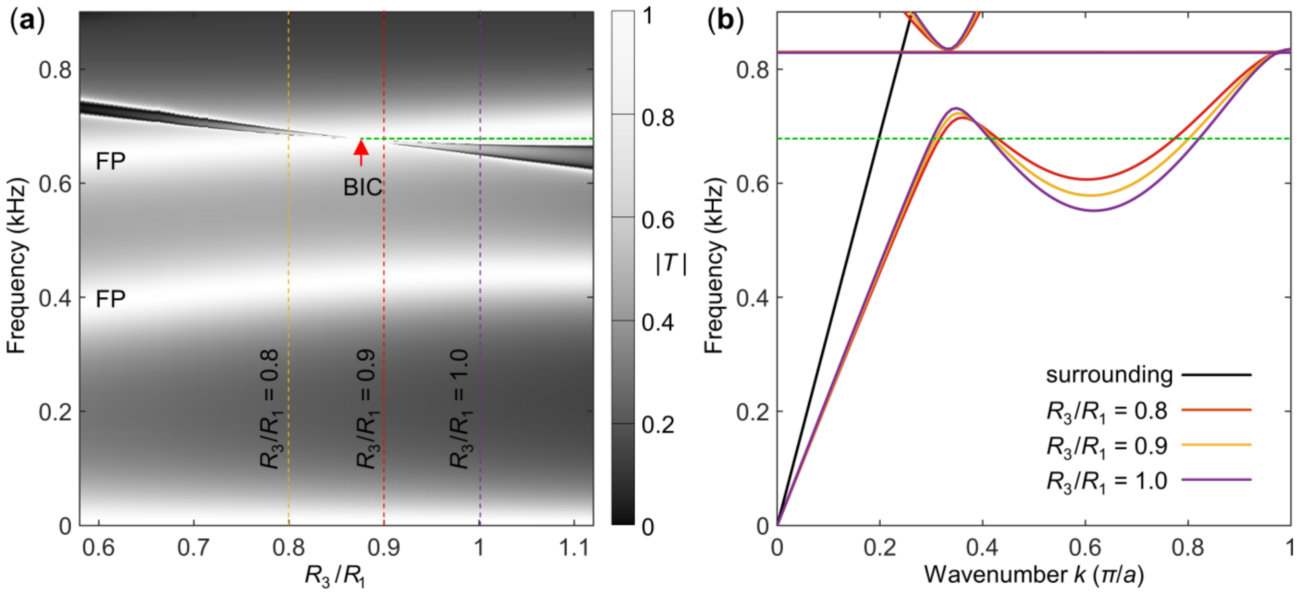

Figure 9. Phonon transmission results of the designed metamaterial. (a) Numerically obtained transmission spectrum $|T|$ for the metamaterial structure shown in Fig. 8(b) versus exciting frequency $\omega/(2\pi)$ and versus the ratio R_3/R_1. Damping is neglected. The bound-states-in-the-continuum (BIC) point is marked by the red arrow. (b) Calculated phonon dispersion relation for three selected ratios R_3/R_1 (see legend). The lowest acoustic band exhibits a pronounced roton-like behavior. For comparison, the dispersion relation of the surrounding (a straight line) is depicted by the black solid curve.

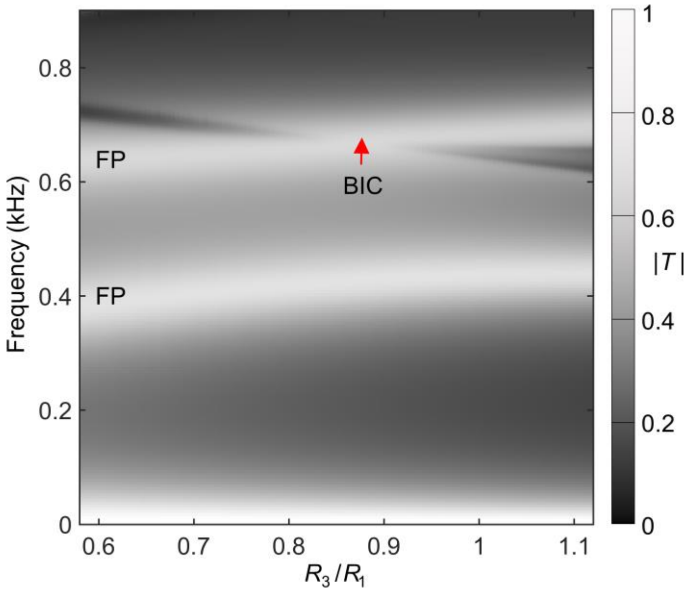

Figure 10. Numerically obtained transmission spectrum $|T|$ with viscous damping in the acoustic pipes is accounted for. As a result, the resonances around the BIC point are smeared out, but the overall qualitative behavior remains unchanged.

References:

1. Liu, Z., et al. Locally resonant sonic materials. *Science* **289**, 1734-1736 (2000).

2. Kadic, M., Milton G. W., van Hecke M. & Wegener M. 3D metamaterials. *Nat. Rev. Phys.* **1**, 198-210 (2019).

3. Frenzel, T., Kadic M. & Wegener M. Three-dimensional mechanical metamaterials with a twist. *Science* **358**, 1072-1074 (2017).

4. Pendry, J. B., Holden A. J., Stewart W. J. & Youngs I. Extremely low frequency plasmons in metallic mesostructures. *Phys. Rev. Lett.* **76**, 4773 (1996).

5. Smith, D. R., Pendry J. B. & Wiltshire M. Metamaterials and negative refractive index. *Science* **305**, 788-792 (2004).

6. Zhu, R., Liu X. N., Hu G. K., Sun C. T. & Huang G. L. Negative refraction of elastic waves at the deep-subwavelength scale in a single-phase metamaterial. *Nat. Commun.* **5**, 5510 (2014).

7. Liu, X. N., Huang G. L. & Hu G. K. Chiral effect in plane isotropic micropolar elasticity and its application to chiral lattices. *J. Mech. Phys. Solids* **60**, 1907-1921 (2012).

8. Chen, Y., Frenzel T., Guenneau S., Kadic M. & Wegener M. Mapping acoustical activity in 3D chiral mechanical metamaterials onto micropolar continuum elasticity. *J. Mech. Phys. Solids* **137**, 103877 (2020).

9. Xu, X., et al. Physical Realization of Elastic Cloaking with a Polar Material. *Phys. Rev. Lett.* **124**, 114301 (2020).

10. Farzbod, F. & Scott-Emuakpor O. E. Interactions beyond nearest neighbors in a periodic structure: Force analysis. *Int. J. Solids Struct.* **199**, 203-211 (2020).

11. Di Paola, M. & Zingales M. Long-range cohesive interactions of non-local continuum faced by fractional calculus. *Int. J. Solids Struct.* **45**, 5642-5659 (2008).

12. Chaplain, G. J., Hooper I. R., Hibbins A. P. & Starkey T. A. Reconfigurable Elastic Metamaterials: Engineering Dispersion with Meccano™. *arXiv preprint arXiv:2206.10487*, (2022).

13. Kutsenko, A. A., Shuvalov, A. L., Poncelet, O. & Darinskii, A. N. Quasistatic stopband and other unusual features of the spectrum of a one-dimensional piezoelectric phononic crystal controlled by negative capacitance. *C. R. Mecanique* **343**, 680-688 (2015).

14. Kutsenko, A. A., Shuvalov, A. L. & Poncelet, O. Dispersion spectrum of acoustoelectric waves in 1D piezoelectric crystal coupled with 2D infinite network of capacitors. *J. Appl. Phys.* **123**, 044902 (2018).

15. Chen, Y., Kadic M. & Wegener M. Roton-like acoustical dispersion relations in 3D metamaterials. *Nat. Commun.* **12**, 3278 (2021).

16. Wang, K., Chen Y., Kadic M., Wang C. & Wegener M. Nonlocal interaction engineering of 2D roton-like dispersion relations in acoustic and mechanical metamaterials. *Commun. Mat.* **3**, 35 (2022).

17. Martínez, J. A. I., et al. Experimental Observation of Roton-Like Dispersion Relations in Metamaterials. *Sci. Adv.* **7**, m2189 (2021).

18. Zhu, Z., et al. Observation of multiple rotons and multidirectional roton-like dispersion relations in

acoustic metamaterials. *New J. Phys.* **24**, 123019 (2022).

19. Landau, L. Theory of the Superfluidity of Helium II. *Phys. Rev.* **60**, 356 (1941).

20. Feynman, R. P. & Cohen M. Energy spectrum of the excitations in liquid helium. *Phys. Rev.* **102**, 1189 (1956).

21. Godfrin, H., et al. Dispersion relation of Landau elementary excitations and thermodynamic properties of superfluid He 4. *Phys. Rev. B* **103**, 104516 (2021).

22. Dietrich, O. W., Graf E. H., Huang C. H. & Passell L. Neutron scattering by rotons in liquid helium. *Phys. Rev. A* **5**, 1377 (1972).

23. Kinsler, L. E., Frey A. R., Coppens A. B. & Sanders J. V. *Fundamentals of acoustics* (Wiley, 1999).

24. Hernández, G. *Fabry-perot interferometers* (Cambridge University Press, 1988).

25. Hsu, C. W., Zhen B., Stone A. D., Joannopoulos J. D. & Soljačić M. Bound states in the continuum. *Nat. Rev. Mat.* **1**, 16048 (2016).

26. Parker, R. & Griffiths W. M. Low frequency resonance effects in wake shedding from parallel plates. *J. Sound Vib.* **7**, 371-379 (1968).

27. Chen, Y., Liu X. & Hu G. Influences of imperfectness and inner constraints on an acoustic cloak with unideal pentamode materials. *J. Sound Vib.* **458**, 62-73 (2019).

28. Haq, O. & Shabanov S. Bound states in the continuum in elasticity. *Wave Motion* **103**, 102718 (2021).

29. Limonov, M. F., Rybin M. V., Poddubny A. N. & Kivshar Y. S. Fano resonances in photonics. *Nat. Photonics* **11**, 543-554 (2017).

30. Marinica, D. C., Borisov A. G. & Shabanov S. V. Bound States in the continuum in photonics. *Phys. Rev. Lett.* **100**, 183902 (2008).

31. Zhou, Q., et al. Geometry symmetry-free and higher-order optical bound states in the continuum. *Nat. Commun.* **12**, 4390 (2021).

32. Kittel, C. *Introduction to solid state physics* (Wiley, 2005).

33. Fleury, R. Non-local oddities. *Nat. Phys.* **17**, 766-767 (2021).

34. Heiss, W. D. The physics of exceptional points. *Journal of physics. A, Mathematical and theoretical* **45**, 444011-444016 (2012).

35. Zhen, B., et al. Spawning rings of exceptional points out of Dirac cones. *Nature* **525**, 354-358 (2015).

36. Rosa, M. I. N., Mazzotti M. & Ruzzene M. Exceptional points and enhanced sensitivity in PT-symmetric continuous elastic media. *J. Mech. Phys. Solids* **149**, 104325 (2021).

37. Hein, S., Koch W. & Nannen L. Fano resonances in acoustics. *J. Fluid Mech.* **664**, 238-264 (2010).

38. Graff, K. F. Wave motion in elastic solids (Courier Corporation, 2012).

39. Kanwal, R. P. *Generalized functions theory and technique: Theory and technique* (Springer Science & Business Media, 1998).

40. Norris, A. N., Shuvalov A. L. & Kutsenko A. A. Analytical formulation of three-dimensional dynamic homogenization for periodic elastic systems. *Proc. R. Soc. A* **468**, 1629-1651 (2012).

41. Chen, W. Q., Bian Z. G. & Ding H. J. Three-dimensional vibration analysis of fluid-filled orthotropic FGM cylindrical shells. *Int. J. Mech. Sci.* **46**, 159-171 (2004).

42. Frenzel, T., David Brehm J., Bückmann T., Schittny R., Kadic M. & Wegener M. Three-dimensional labyrinthine acoustic metamaterials. *Appl. Phys. Lett.* **103**, 61907 (2013).

43. Berenger, J. A perfectly matched layer for the absorption of electromagnetic waves. *J. Comput. Phys.* **114**, 185-200 (1994).